JBC RESEARCH ARTICLE

Substrate-binding loop interactions with pseudouridine trigger conformational changes that promote catalytic efficiency of pseudouridine kinase PUKI

Received for publication, November 17, 2021, and in revised form, March 21, 2022 Published, Papers in Press, March 26, 2022,
https://doi.org/10.1016/j.jbc.2022.101869

Sang-Hoon Kim[1], **Minjeong Kim**[2], **Daechan Park**[2,3], **Sujeong Byun**[1], **and Sangkee Rhee**[1,4,*]

From the [1]*Department of Agricultural Biotechnology, Seoul National University, Seoul, Korea;* [2]*Department of Molecular Science & Technology, and* [3]*Department of Biological Sciences, Ajou University, Suwon, Korea;* [4]*Research Institute of Agriculture and Life Sciences, Seoul National University, Seoul, Korea*

Edited by Wolfgang Peti

Pseudouridine, one major RNA modification, is catabolized into uracil and ribose-5′-phosphate by two sequential enzymatic reactions. In the first step, pseudouridine kinase (PUKI) phosphorylates pseudouridine to pseudouridine 5′-monophosphate. High-fidelity catalysis of pseudouridine by PUKI prevents possible disturbance of *in vivo* pyrimidine homeostasis. However, the molecular basis of how PUKI selectively phosphorylates pseudouridine over uridine with >100-fold greater efficiency despite minor differences in their K_m values has not been elucidated. To investigate this selectivity, in this study we determined the structures of PUKI from *Escherichia coli* strain B (EcPUKI) in various ligation states. The structure of EcPUKI was determined to be similar to PUKI from *Arabidopsis thaliana*, including an α/β core domain and β-stranded small domain, with dimerization occurring *via* the β-stranded small domain. In a binary complex, we show that Ser30 in the substrate-binding loop of the small domain mediates interactions with the hallmark N1 atom of pseudouridine nucleobase, causing conformational changes in its quaternary structure. Kinetic and fluorescence spectroscopic analyses also showed that the Ser30-mediated interaction is a prerequisite for conformational changes and subsequent catalysis by EcPUKI. Furthermore, S30A mutation or EcPUKI complexed with other nucleosides homologous to pseudouridine but lacking the pseudouridine-specific N1 atom did not induce such conformational changes, demonstrating the catalytic significance of the proposed Ser30-mediated interaction. These analyses provide structural and functional evidence for a pseudouridine-dependent conformational change of EcPUKI and its functional linkage to catalysis.

RNA modifications have been recognized in noncoding RNAs and tRNAs and are also present in various coding RNAs (1, 2). They have important roles in the maintenance of stability for tRNAs (3–5) and mRNAs (5) and in the regulation of the translation efficiency of mRNAs (6, 7). Their biological effects are diverse. For example, RNA modifications in humans and yeast are regulated in response to changes in the environment (8, 9). Among more than 140 RNA modifications identified in all organisms, N^6-methylated adenine and pseudouridine (Ψ), a C5-glycoside isomer of uridine (Fig. 1*A*), are the most prevalent (10, 11). The biogenesis of these modifications and their biological effects are reviewed elsewhere (1, 2, 5).

The catabolic fates of N^6-methylated adenine (12) and pseudouridine are emerging from studies of noncanonical nucleotides derived from modification-containing RNAs. In particular, pseudouridine catabolism was first suggested in pyrimidine auxotrophic *Escherichia coli* mutants (13). Thirty-eight years later, two enzymes in the pathway—YeiC and YeiN—were identified (14). Details regarding pseudouridine catabolism, with its physiological consequences, were gleaned from studies of *Arabidopsis* (15). A lack of high sequence conservation from *E. coli* to eukaryotes hampered the identification of genes involved in pseudouridine catabolism within *Arabidopsis thaliana*. The metabolic turnover of pseudouridine-containing RNAs in vacuole produces pseudouridine monophosphate, which is dephosphorylated and exported to the peroxisome *via* the cytosol. In the peroxisome, pseudouridine is converted into uracil and ribose-5′-phosphate by two consecutive reactions that correspond to the activities of YeiC and YeiN, respectively, from *E. coli*. Therefore, the pseudouridine catabolic pathway recycles metabolic intermediates of uracil and ribose-5′-phosphate for use in other metabolic pathways.

Pseudouridine kinase (PUKI), a member of the phosphofructokinase B (PfkB) family (16), catalyzes the first of the two consecutive reactions (15). PUKI phosphorylates pseudouridine to pseudouridine 5′-monophosphate in an ATP-dependent manner (Fig. 1*A*); in the second step, pseudouridine 5′-monophosphate is hydrolyzed into uracil and ribose-5′-phosphate by pseudouridine monophosphate glycosylase. Recently, we performed a structural analysis of PUKI from *A. thaliana* (AtPUKI) and disclosed the structural basis for its substrate specificity toward pseudouridine (17). The enzyme efficiency (*i.e.*, k_{cat}/K_m) was 100-fold greater for pseudouridine than for structurally homologous uridine, despite minor differences in their K_m values. These observations led us to postulate that AtPUKI catalytically distinguishes

* For correspondence: Sangkee Rhee, srheesnu@snu.ac.kr.

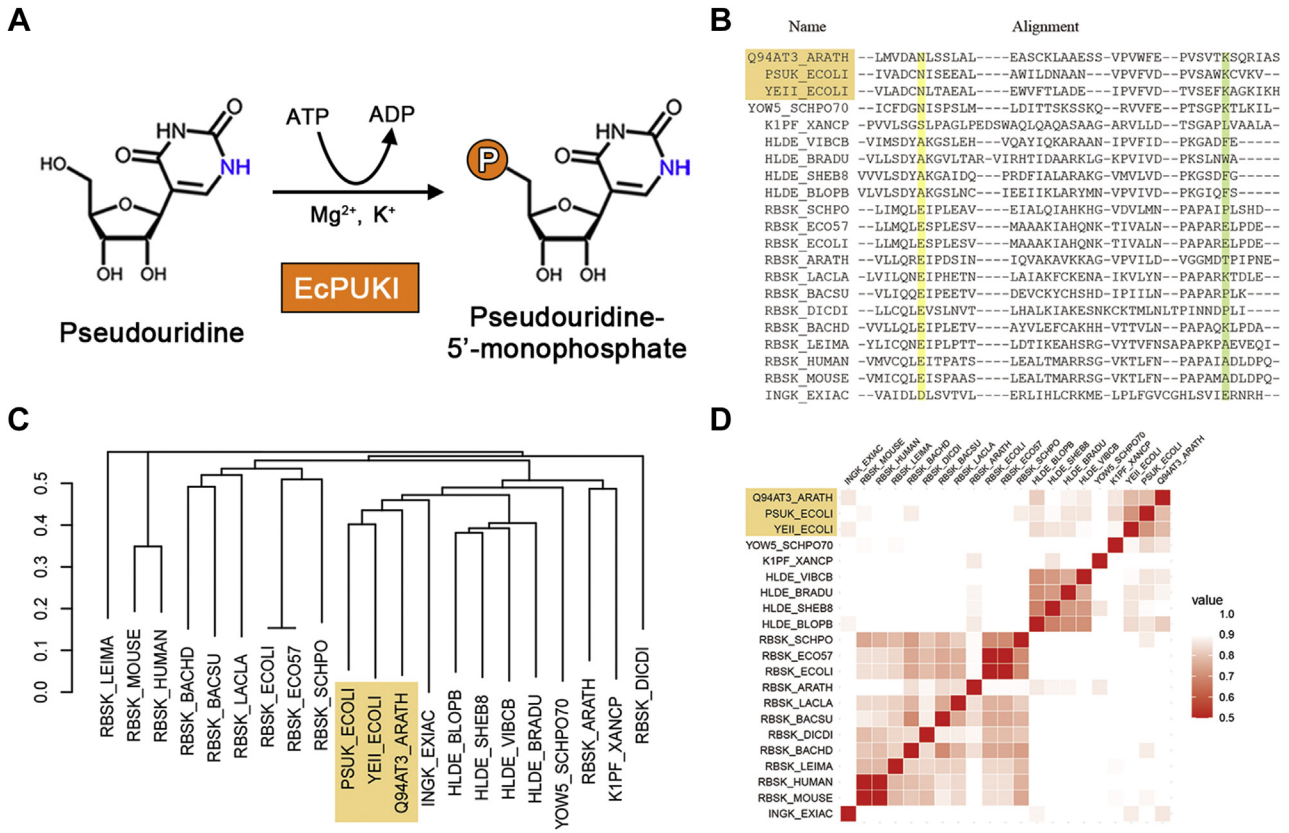

Figure 1. Reaction scheme and phylogenetic comparison of PUKIs. *A*, in *Escherichia coli*, PUKI catalyzes the phosphorylation of pseudouridine using ATP as a phosphate donor, yielding pseudouridine 5′-monophosphate and ADP. *B*, MSA of local amino acid sequences including two hydrophilic active site residues for the top 20 highly homologous proteins to AtPUKI. Q94AT3_ARATH and PSUK_ECOLI refer to AtPUKI and EcPUKI, respectively. The function of *E. coli* YeiI is uncharacterized. Other homologs are described in the Experimental procedures section. *C*, phylogenetic tree of homologs of MSA constructed using the neighbor-joining method. *D*, heat map of pairwise distances of MSA. AtPUKI, PUKI from *Arabidopsis thaliana*; EcPUKI, PUKI from *Escherichia coli* strain B; MSA, multiple sequence alignment; PUKI, pseudouridine kinase.

pseudouridine from uridine possibly by pseudouridine-induced conformational changes.

Here, we conducted a structural analysis of PUKI from *E. coli* strain B (EcPUKI) in the absence or the presence of pseudouridine, uridine, or cytidine. We also performed kinetic and fluorescence spectroscopic analyses. These findings provide structural and functional evidence concerning the pseudouridine-dependent conformational change in PUKI and its functional linkage to catalysis.

Results and discussion

Phylogenetic analysis of PUKIs in the PfkB proteins

The sequence identity of full-length EcPUKI and AtPUKI is low (21%). We therefore investigated the evolutionary relationship of PUKIs in PfkB proteins using local structural information for AtPUKI (17). Before the construction of a phylogenetic tree, AtPUKI homologs were identified using the BLAST (18) by querying the full-length AtPUKI. The top 20 proteins ranked by similarity score were subjected to homology modeling in SWISS-MODEL (19) using AtPUKI (Protein Data Bank [PDB] ID: 7C1X) as the template. This modeling allowed us to identify the ligand-binding region with two hydrophilic active site residues; those residues correspond to positions 137 and 166 in AtPUKI, which are crucial for pseudouridine affinity (17). Multiple sequence alignment (MSA) was performed using amino acid sequences containing the two active site residues (20). This demonstrated the conservation of N (Asn) and K (Lys) in EcPUKI and AtPUKI (Fig. 1*B*). Notably, phylogenetic analysis revealed that EcPUKI and AtPUKI, together with *E. coli* YeiI, whose function is unknown, are evolutionarily closer than other PfkB proteins, such as ribokinases (RBSKs) (Fig. 1*C*). Pairwise distances for the alignments confirmed that functionally equivalent PfkB family proteins (ortholog) exhibit high sequence identities (Fig. 1*D*). The active site regions of PUKI were conserved between *E. coli* and *A. thaliana*, although the full sequences were phylogenetically distant. Therefore, EcPUKI and AtPUKI are homologous based on the similarity of two active site residues and the local structure.

Structure of EcPUKI in the absence of substrate

In the crystal structure of unliganded EcPUKI at 2.15 Å resolution, the asymmetric unit of the space group *P3* has two dimers (Table 1). The dimerization of EcPUKI in solution was

Table 1
Data collection and refinement statistics

Dataset	Unliganded EcPUKI	EcPUKI–Ψ	EcPUKI–uridine	EcPUKI–cytidine	S30A–Ψ
PDB ID	7VTD	7VVA	7VTE	7VTF	7VTG
Data collection					
Crystal	Native	Native	Native	Native	Native
Wavelength (Å)	0.97934	0.97932	0.97932	0.97932	0.97932
Resolution (Å)	50.0–2.15 (2.23–2.15)[a]	50.0–2.75 (2.85–2.75)	50.0–2.15 (2.23–2.15)	50.0–2.20 (2.28–2.20)	50.0–1.90 (1.97–1.90)
Unique reflections	104,842	92,181	104,992	99,598	155,963
Multiplicity	5.4 (5.2)	3.5 (3.5)	5.5 (5.3)	5.3 (4.9)	5.2 (4.7)
Completeness (%)	99.7 (100)	99.7 (99.8)	99.7 (100)	99.8 (100)	99.6 (100)
Mean I/sigma(I)	15.0 (0.89)	7.7 (1.0)	12.7 (0.69)	13.0 (0.57)	15.3 (0.84)
Wilson *B*-factors (Å^2)	49.6	52.8	52.9	54.3	35.7
R_{merge}[b]	0.13 (1.76)	0.20 (1.98)	0.15 (2.41)	0.14 (2.47)	0.11 (1.84)
$CC_{1/2}$[c]	0.99 (0.50)	0.95 (0.34)	0.98 (0.45)	0.99 (0.49)	0.96 (0.43)
Space group	*P3*	$P2_1$	*P3*	*P3*	*P3*
Unit cell *a*, *b*, *c* (Å)	186.8, 186.8, 49.7	72.0, 271.9, 101.2	185.7, 185.7, 50.8	186.0, 186.0, 51.0	185.1, 185.1, 51.7
α, *β*, *γ* (°)	90.0, 90.0, 120.0	90.0, 110.9, 90.0	90.0, 90.0, 120.0	90.0, 90.0, 120.0	90.0, 90.0, 120.0
Refinement					
R_{work}[d] (%)	23.2	29.6	25.0	24.9	21.9
R_{free}[e] (%)	26.8	32.5[f]	28.7	29.8	26.2
No. of atoms	9444	15,795	9155	9110	9498
Macromolecules	9240	15,693	9047	9010	8993
Ligands	—	68	68	68	68
Water	204	34	38	32	437
RMS (bonds) (Å)	0.004	0.003	0.005	0.004	0.018
RMS (angles) (°)	0.905	0.802	1.029	1.013	1.662
Ramachandran					
Favored (%)	97.1	92.9	96.7	97.8	97.2
Outliers (%)	0.2	1.2	0.00	0.17	0.00
Average *B*-factor (Å^2)	86.0	69.1	93.4	88.8	56.5
Macromolecules	86.4	69.1	93.4	88.7	56.8
Ligands	—	52.5	102.4	96.4	43.8
Water	68.0	42.9	73.0	66.7	56.7

[a] Numbers in parentheses refer to data in the highest resolution shell.
[b] $R_{merge} = \Sigma I_h - \langle I_h \rangle | / \Sigma I_h$, where I_h is the observed intensity and $\langle I_h \rangle$ is the average intensity.
[c] The $CC_{1/2}$ is the Pearson correlation coefficient (CC) calculated from each subset containing a random half of the measurements of unique reflection.
[d] $R_{work} = \Sigma ||F_{obs}| - |F_{cal}|| / \Sigma |F_{obs}|$.
[e] R_{free} is the same as R_{obs} for a selected subset (5%) of the reflections that was not included in prior refinement calculations.
[f] R_{free} of the EcPUKI–Ψ binary complex is relatively high because some of the monomers are suffered from poor density.

characterized by size-exclusion chromatography (Fig. 2*A*). Therefore, the dimer is a biological functional unit. From a structural perspective, the four protomers in the two dimers are essentially identical, with an RMSD of 0.19 to 0.21 Å for about 307 Cα atoms.

Monomeric EcPUKI (Glu3 to Ala309) exhibits an α/β Rossmann fold, a typical structure for PfkB proteins (16). EcPUKI, with 11 α-helices and 14 β-strands, is folded into an α/β core domain, with a protruding four β-stranded small domain (Figs. 2, *B* and *C*, S1). In the core domain, 10 β-strands form the central β-sheet, in the order β6–β5–β4–β1–β9–β10–β11–β12–β13–β14. These β-strands are parallel, except for β13. The β-stranded small domain, which comprises β2, β3 and β7, β8, is bent toward the α/β core domain, forming a substrate-binding pocket between the two domains (see the subsection *Pseudouridine-induced conformational changes*). The β-stranded small domains of the two subunits are responsible for dimerization of EcPUKI (Fig. 2*D*) by forming a β-clasp motif; this motif was first characterized in RBSK of *E. coli* (EcRBSK), a member of the PfkB family (21). In particular, a loop in β2–β3 (*green* in Fig. 2*D*; His22 to Pro32, including Ser30, in Fig. S1) in a small domain of one subunit (*orange*) transverses into the substrate-binding pocket of the adjacent subunit (*gray*), forming the substrate-binding loop for catalysis.

These structural features are comparable to the features of AtPUKI, including the substrate-binding loop. A structural homology search using program DALI (22) indicated that a monomeric EcPUKI exhibited high similarity to AtPUKI (PDB ID: 7C1Y; Z-score, 39.2; sequence identity, 21%; and RMSD of 1.76 Å for the 267 Cα atoms) (17), EcRBSK (PDB ID: 1RKA; Z-score, 39.4; sequence identity, 22%; and RMSD of 1.57 Å for the 281 Cα atoms) (23), and RBSK from *A. thaliana* (PDB ID: 6ILT; Z-score, 38.7; sequence identity, 21%; and RMSD of 1.80 Å for the 290 Cα atoms) (24). In a previous structural and kinetic study of AtPUKI (17), we proposed that pseudouridine-induced conformational changes are required for catalysis. Those changes in conformation likely cause two substrates, pseudouridine and ATP, to be properly oriented for a kinase reaction. However, the proposed structural features were not unraveled in a ternary complex of AtPUKI with pseudouridine and ADP; only minor changes were identified (17), compared with the large conformational changes in EcRBSK (21, 23). Analogous to EcRBSK and AtPUKI, we also adopted the Cα-interatomic distance as an indicator of conformational changes. Ser200, which is located at the edge of the core domain, was selected as the indicator residue (Fig. 2*D*). In unliganded EcPUKI, the Cα-interatomic distance between Ser200 and Ser200* (*asterisk* indicates a residue or an element from an adjacent subunit) in the two subunits was approximately 66 Å.

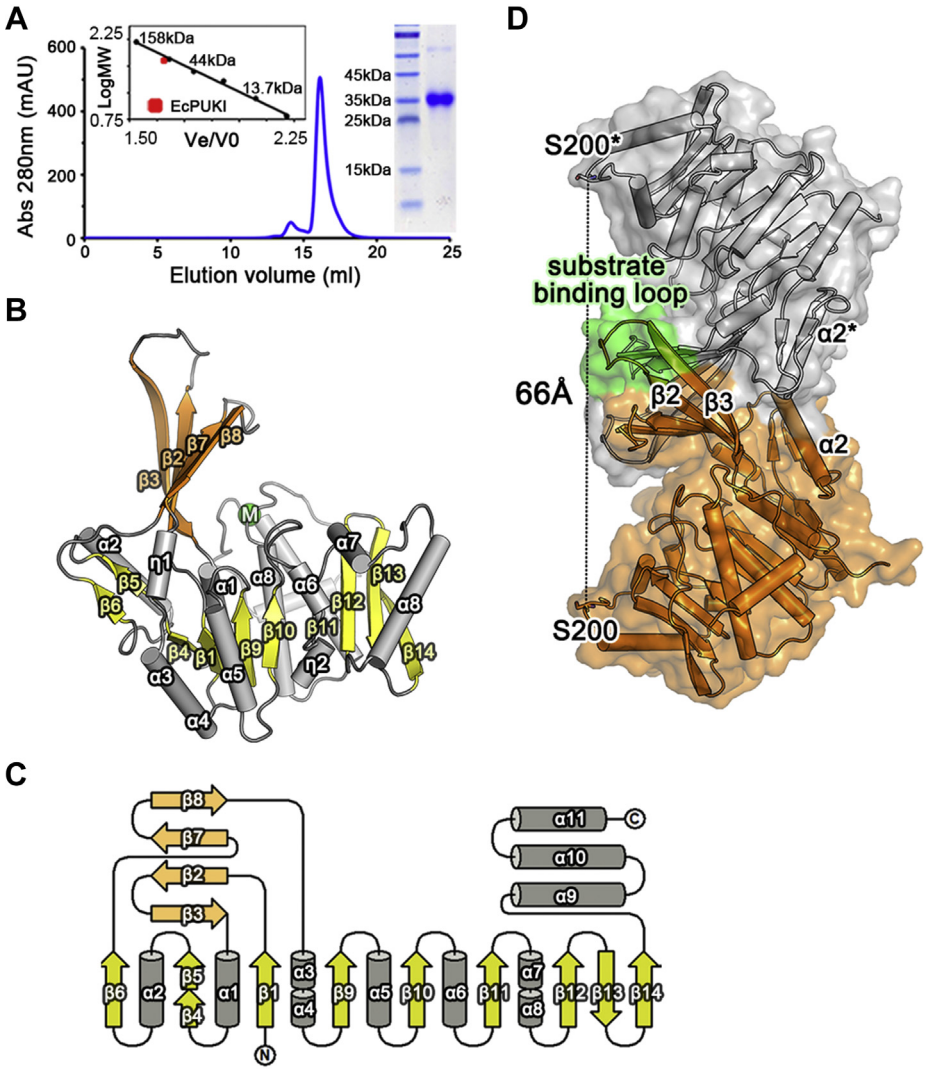

Figure 2. Overall structure of monomeric and dimeric EcPUKI. *A*, size-exclusion chromatographic and SDS-PAGE analyses. EcPUKI was eluted on a Superdex 200 column (Cytiva) with a buffer containing 50 mM phosphate and 150 mM KCl (pH 7.2). The elution peak for EcPUKI indicates a molecular weight of approximately 75 kDa, corresponding to dimeric EcPUKI. *Left inset*, 6.5 to 158 kDa molecular weight markers (Cytiva). *Right inset*, SDS-PAGE of monomeric EcPUKI. *B*, monomeric structure of unliganded EcPUKI is shown. An α/β core domain is shown, with the central β-sheet in *yellow*, flanking α-helices in *gray*, and the β-stranded small domain in *orange*. The monovalent cation-binding site is indicated by a *green circle* with the letter M. The secondary structural elements in Fig. S1 are labeled. *C*, topology of EcPUKI. The color codes and secondary structural elements are identical to those of *B*. *D*, side view of dimeric unliganded EcPUKI with a surface representation. The β-stranded small domain of each subunit mediates dimerization; a substrate-binding loop (*green*) of the small domain transverses into an adjacent subunit (*gray*). The Cα-interatomic distance between Ser200 in each monomer was approximately 66 Å. EcPUKI, pseudouridine kinase from *Escherichia coli* strain B.

Pseudouridine-induced conformational changes

The 2.75 Å resolution crystal structure of EcPUKI complexed with pseudouridine provides structural evidence for conformational changes upon binding of pseudouridine (Fig. 3*A*). This binary structure, which has eight monomers in the asymmetric unit of the space group $P2_1$ (Table 1), exhibits two features. In each dimer, pseudouridine is present in only one subunit (*gray* in Fig. 3*A*). The other subunit shows a highly disordered structure in some regions. In particular, two pseudouridine-unbound subunits among the eight monomers had a disordered electron density. However, the Cα tracing in the other subunits was reliable. In an overall structure of the binary complex, the Cα-interatomic distance indicator was ∼51 Å (Fig. 3*A*), compared with ∼66 Å for unliganded EcPUKI, revealing global conformational changes upon binding of pseudouridine. These changes in quaternary structure are attributable to the β-stranded small domain, rather than the α/β core domain. The structural superposition of the corresponding subunit in unliganded EcPUKI and its binary complex resulted in an RMSD of 0.5 Å for 251 Cα atoms for the α/β core domain. Large structural differences are associated with the β-stranded small domain, with positional changes of up to approximately 9 Å in the substrate-binding loop between the corresponding Cα atoms (Fig. S2). Thus, the β-stranded small domain in a binary complex is more bent toward the α/β core domain, compared with that of unliganded EcPUKI. In dimeric EcPUKI, these dynamic features of the β-stranded small domain result in global conformational changes upon binding of pseudouridine, effectively sealing off pseudouridine for catalysis.

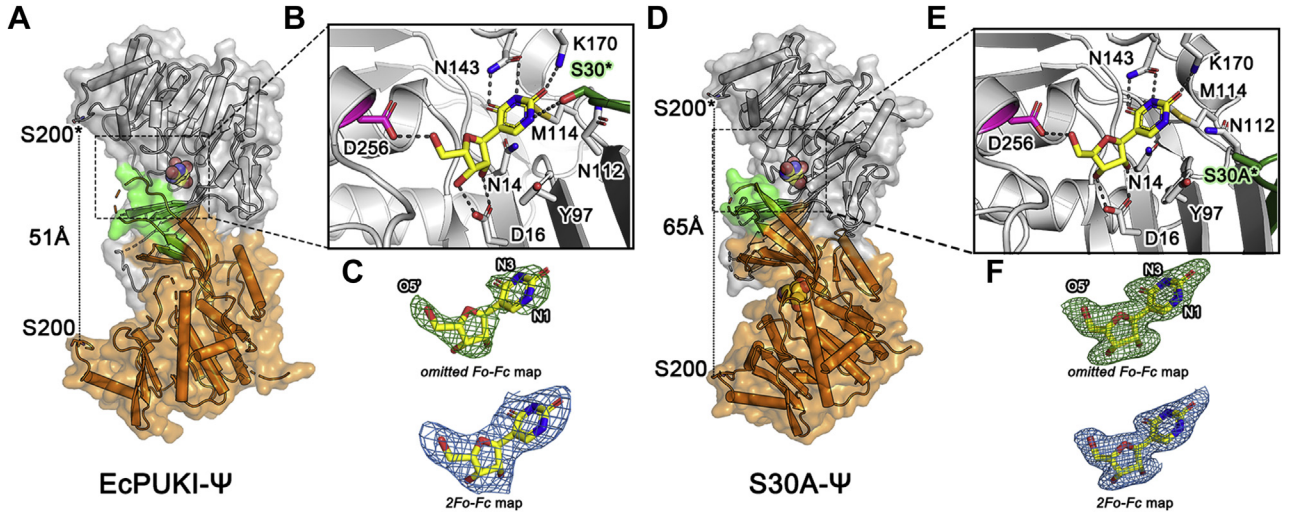

Figure 3. Structural insights into the binary complex of wildtype EcPUKI and S30A mutant with pseudouridine. The overall structure of the binary complex, ligand-binding environment, and ligand electron density are shown. Structural insights into the binary complex of (*A–C*) wildtype EcPUKI and (*D–E*) the S30A mutant. *A*, dimeric EcPUKI with pseudouridine (Ψ), with surface representation, is displayed in a side view similar to Figure 2*D*. Pseudouridine in a space-filling model is buried but can be seen because of the transparency of EcPUKI. The Cα-interatomic distance indicator is ∼51 Å. Note that the substrate-binding loop was buried, compared with unliganded EcPUKI and a binary complex of S30A mutant with pseudouridine in (*D*). *B*, zoom-in view for the binding environment of pseudouridine in a binary complex. Color codes are identical to the codes in (*A*), with Asp256 (*magenta*) as a putative catalytic base. *Dashed lines* indicate possible hydrogen bonds within 3.0 Å. Ser30* in the substrate-binding loop of an adjacent subunit is a part of the substrate-binding pocket. *C*, electron density of pseudouridine in the binary complex, with an omitted *Fo–Fc* and a *2Fo–Fc* electron density map contoured at 3.0 and 1.0 σ, respectively. *D*, overall structure. *E*, zoom-in view for the binding environment of pseudouridine. and *F*, electron density of pseudouridine in the S30A mutant with an omitted *Fo–Fc* and a *2Fo–Fc* electron density map contoured at 3.0 and 1.0 σ, respectively. Global conformational changes were not observed in the binary complex of the S30A mutant with pseudouridine, with ∼65 Å for the Cα-interatomic distance indicator. EcPUKI, pseudouridine kinase from *Escherichia coli* strain B.

Pseudouridine in the binary complex is located in a cleft between the β-stranded small domain and the concave side of the α/β core domain (Fig. 3, *B* and *C*), with its nucleobase (hereafter referred to as uracil-Ψ) pointing toward the substrate-binding loop (*green* in Fig. 3*B*). Specifically, the ribosyl moiety forms several interactions within ∼3.3 Å with nearby residues: Asp16 with O2′ and O3′; Asn14 with O2′; and Asp256, a proposed catalytic base, with O5′, to which the γ-phosphate group of ATP is attached. The uracil-Ψ moiety is surrounded by Tyr97, Asn112, and Met114 on one side and by the hydrophilic residues Ser30*, Asn143, and Lys170 (Fig. 3*B*). There are possible hydrogen bonds within ∼3.5 Å around the uracil-Ψ moiety: N3 and O4 of the base with Asn143 *via* bidentate interactions, O2 with Lys170, and N1 with Ser30*, a residue of the substrate-binding loop of the adjacent subunit.

Considering crystal packing interactions could affect the conformational state(s) of EcPUKI, we analyzed those packing interactions of unliganded EcPUKI in the *P3* space group and in a binary complex with pseudouridine in the $P2_1$ space group (Table 1). In the PISA (Protein Interfaces, Surfaces and Assemblies) analysis (25), the interface area for crystal packing around a particular monomer was calculated. Although the two space groups had similar interface area values (2894 Å^2 for *P3* and 2737 Å^2 for $P2_1$), a small number of crystal contacts in the critical regions could affect the conformational freedom of molecules. Therefore, we still cannot rule out the possible effects of crystal contacts on the changes in EcPUKI conformation. Consistent with the crystal structure of EcPUKI complexed with pseudouridine, further structural analysis, mutagenesis, and fluorescence spectroscopy of various EcPUKIs in the current study unanimously support the pseudouridine-induced conformational changes of EcPUKI.

Catalysis of EcPUKI

The binding environment of pseudouridine in EcPUKI is comparable to that of pseudouridine in AtPUKI (17). In AtPUKI, there are variations in the hydrophobic residues around the uracil-Ψ moiety, but three hydrophilic residues were identified: Asn137^{AtPUKI}, Lys166^{AtPUKI}, and Thr26^{AtPUKI} (superscript AtPUKI indicates residue(s) in AtPUKI) (Fig. 1*B*). Three residues, which differ in Thr26^{AtPUKI} and Ser30^{EcPUKI}, are hallmarks of PUKI family proteins.

EcPUKI residues interacting with a uracil-Ψ have crucial roles in enzyme activity. For a functional analysis, we validated that the monovalent cation K^+, the divalent cation Mg^{2+}, and a phosphate donor ATP are required for EcPUKI activity, with high specificity for pseudouridine and no requirement for inorganic phosphate as an activator (Fig. 4, *A–E*). Specific activity measurements of mutants demonstrated that residues around pseudouridine have various effects on enzyme activity (Figs. 3*B* and 5*A*). Among them, the mutation of three hydrophilic residues around the uracil-Ψ moiety—Ser30, Asn143, and Lys170—resulted in catalytically incompetent enzymes, with activities of 0.1 to 5.5% of the wildtype enzyme (Fig. 5*A*). Therefore, the possible hydrogen bonds mediated by these three residues have central roles in the kinase activity of EcPUKI. Steady-state kinetic analyses yielded supporting evidence (Fig. 5, *B* and *C*). Mutation of the uracil-Ψ-interacting residues (Y97A, N112A, and M114A) and the three hydrophilic residues (S30A, N143A, and K170A) increased the K_m value by

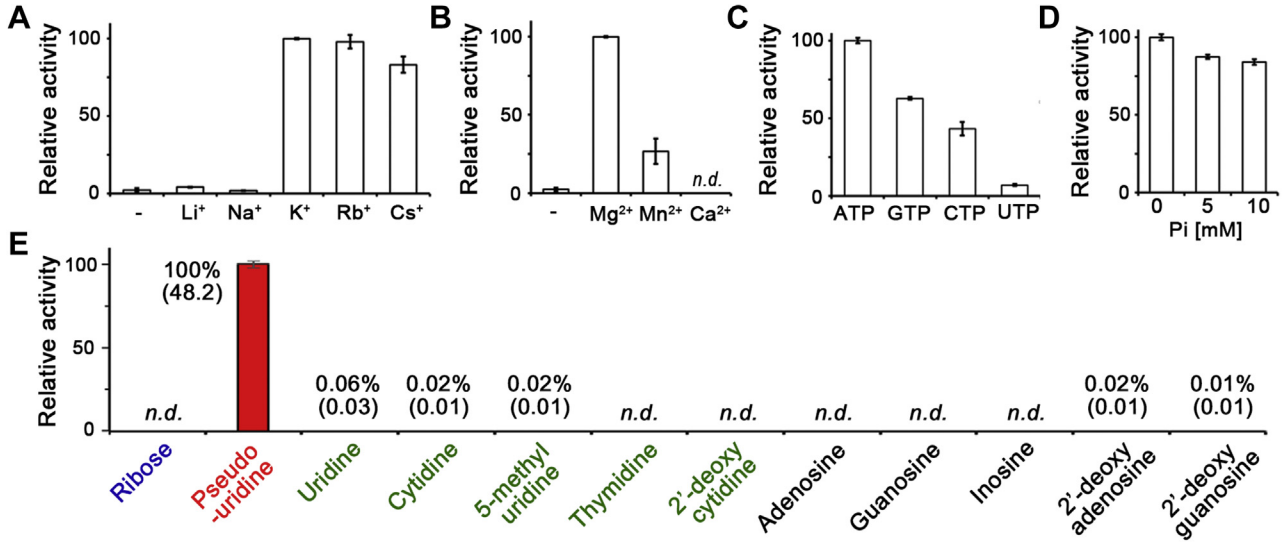

Figure 4. Effects of cations, nucleoside triphosphates, inorganic phosphate, and nucleosides on EcPUKI activity. The relative activity using a direct activity assay was measured with (*A*) 50 mM monovalent cations, (*B*) 20 mM divalent cations, and (*C*) 1 mM nucleoside triphosphates as phosphate donors. *D*, an enzyme-coupled assay was employed to evaluate the effect of phosphate on EcPUKI activity. The mean value of the highest measurements was set to 100%. Error bars are standard deviations (n = 3). *E*, substrate specificity of EcPUKI for nucleosides (1.25 mM) under ATP saturation conditions (4 mM ATP). Activities were compared with wildtype EcPUKI (48.2 μmol min^{-1} mg^{-1} protein set to 100%; Fig. 5*A*). Consistent with PUKI of *E. coli* K-12 (14), EcPUKI showed high specificity for pseudouridine, with negligible activities for other potential substrates, including similar pyrimidine nucleosides (uridine, cytidine, 5′-methyluridine, thymidine, and 2′-deoxycytidine). EcPUKI, pseudouridine kinase from *Escherichia coli* strain B; n.d., not detected.

approximately 1.4- to 55.1-fold, and their k_{cat} values are in a range of 0.087 to 109%, compared with wildtype EcPUKI. The enzyme efficiency (*i.e.*, k_{cat}/K_m) of the mutants was therefore 0.06 to 31% of wildtype EcPUKI. Mutant S30A showed the lowest efficiency for pseudouridine (0.06% of wildtype EcPUKI). Unlike the N143A and K170A mutants showing 55- and 11-fold increased K_m values, respectively, the S30A mutant had a significantly reduced k_{cat} value (0.087% of wildtype EcPUKI), but its K_m value is only a 1.4-fold increase.

Functional role of Ser30 in the substrate-binding loop

The substrate-binding loop containing Ser30 has dynamic structural features that enable the pseudouridine-induced

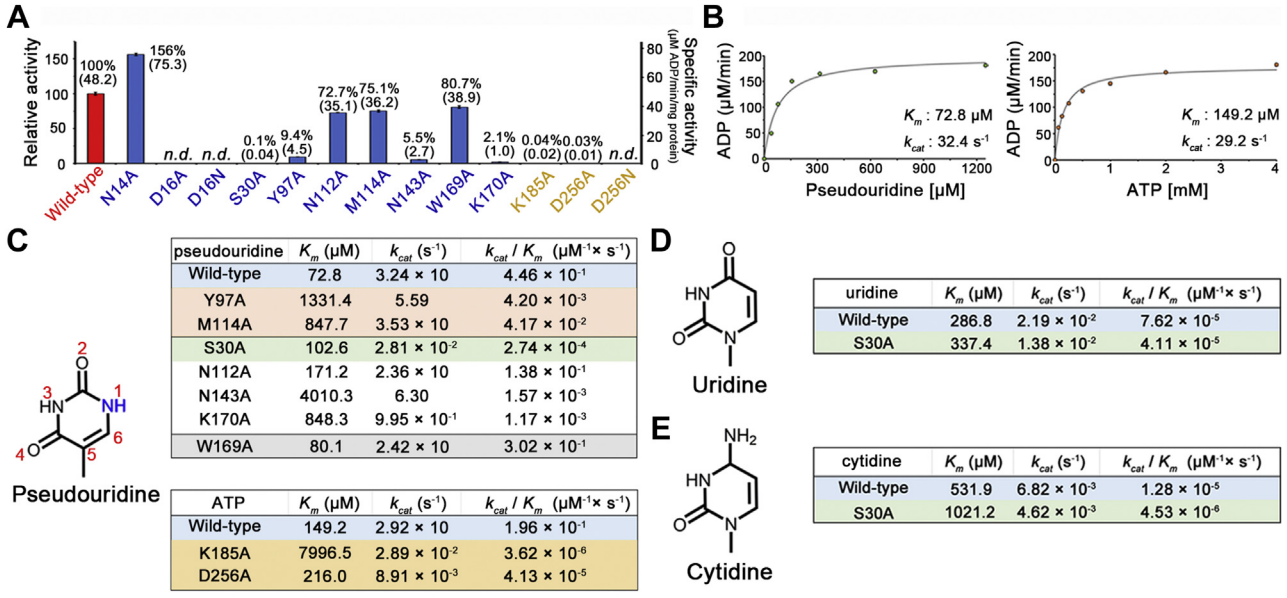

pseudouridine	K_m (μM)	k_{cat} (s^{-1})	k_{cat} / K_m ($μM^{-1}$× s^{-1})
Wild-type	72.8	3.24 × 10	4.46 × 10^{-1}
Y97A	1331.4	5.59	4.20 × 10^{-3}
M114A	847.7	3.53 × 10	4.17 × 10^{-2}
S30A	102.6	2.81 × 10^{-2}	2.74 × 10^{-4}
N112A	171.2	2.36 × 10	1.38 × 10^{-1}
N143A	4010.3	6.30	1.57 × 10^{-3}
K170A	848.3	9.95 × 10^{-1}	1.17 × 10^{-3}
W169A	80.1	2.42 × 10	3.02 × 10^{-1}

ATP	K_m (μM)	k_{cat} (s^{-1})	k_{cat} / K_m ($μM^{-1}$× s^{-1})
Wild-type	149.2	2.92 × 10	1.96 × 10^{-1}
K185A	7996.5	2.89 × 10^{-2}	3.62 × 10^{-6}
D256A	216.0	8.91 × 10^{-3}	4.13 × 10^{-5}

uridine	K_m (μM)	k_{cat} (s^{-1})	k_{cat} / K_m ($μM^{-1}$× s^{-1})
Wild-type	286.8	2.19 × 10^{-2}	7.62 × 10^{-5}
S30A	337.4	1.38 × 10^{-2}	4.11 × 10^{-5}

cytidine	K_m (μM)	k_{cat} (s^{-1})	k_{cat} / K_m ($μM^{-1}$× s^{-1})
Wild-type	531.9	6.82 × 10^{-3}	1.28 × 10^{-5}
S30A	1021.2	4.62 × 10^{-3}	4.53 × 10^{-6}

Figure 5. Mutational and kinetic analyses of EcPUKIs. *A*, specific activity of EcPUKIs. *Red*, wildtype; *blue*, pseudouridine-binding pocket mutants; and *yellow*, mutants for possible catalytic residues. The specific activities in parentheses were compared with wildtype EcPUKI (48.2 μmol min^{-1} mg^{-1} protein set to 100%). Each measurement was conducted in triplicate; error bars indicate standard deviations. Activity assays were performed as described (17). ADP production was monitored for 30 s under substrate saturation conditions (4 mM ATP and 1.25 mM pseudouridine) for wildtype EcPUKI. *B*, steady-state kinetic analyses of EcPUKI with pseudouridine and ATP as substrates. Error bars are standard deviations (n = 3). Kinetic analyses involved 4 mM ATP or 1.25 mM pseudouridine with 100 nM EcPUKI. *C–E*, steady-state kinetic parameters of the mutants. Kinetic assays of phosphate acceptors (pseudouridine, uridine, and cytidine) were conducted in the presence of 4 mM ATP. The kinetic assay for ATP in Figure 5*C* was performed in the presence of 1.25 mM pseudouridine. Concentrations of EcPUKI are in a range of 100 nM–24 μM. EcPUKI, pseudouridine kinase from *Escherichia coli* strain B; n.d., not detected.

conformational changes (Figs. 3*A* and S2). Considering the significant reduction of the k_{cat}, but not the K_m, value of the S30A mutant (Fig. 5*C*), we propose that Ser30-mediated interaction between a substrate-binding loop and uracil-Ψ constitutes a prerequisite for conformational changes and catalysis by EcPUKI. Therefore, the effects of the S30A mutation likely result from an inability to undergo the conformational changes required for activity.

We performed a structural analysis of EcPUKI to validate the proposed function of Ser30. Indeed, the 1.90 Å resolution crystal structure of S30A complexed with pseudouridine did not show global conformational changes (Fig. 3*D* and Table 1; distance indicator of ∼65 Å, similar to unliganded EcPUKI). Pseudouridine is present in both subunits, unlike the wildtype enzyme and its binding environment in the S30A mutant is reminiscent of that of wildtype EcPUKI (Fig. 3, *E* and *F*). However, because of the Ser30 to Ala30 mutation, there is no interaction within ∼7 Å between Ala30 and the N1 of uracil-Ψ, restricting movement of the β-stranded small domain and its adoption of an orientation identical to unliganded EcPUKI. Next, we determined the structure of wildtype EcPUKI complexed with uridine or cytidine (Fig. S3 and Table 1) at 2.15 and 2.20 Å resolution, respectively, which do not interact with Ser30 because of the absence of the hallmark uracil-Ψ N1 atom in the nucleobases (Fig. 5, *D* and *E*). Those ligands, which are structurally homologous to pseudouridine, bound within a pseudouridine-binding cleft in an almost identical manner to wildtype EcPUKI complexed with pseudouridine. However, they did not induce conformational changes (Fig. S3). These structural features are correlated with the kinetic parameters of wildtype EcPUKI and S30A mutant for uridine and cytidine (Fig. 5, *D* and *E*), with a 1500- to 7000-fold reduction in k_{cat} and a 4- to 14-fold increase in K_m, compared with wildtype EcPUKI for pseudouridine. Therefore, the conformational changes in EcPUKI induced by the binding of pseudouridine to a substrate-binding loop *via* Ser30 are essential for activity.

Conformational changes of EcPUKI in solution

We further investigated substrate-induced conformational changes of EcPUKI in solution using intrinsic fluorescence measurements. Using an excitation wavelength of 289 nm, the emission spectra of EcPUKI in the presence of various ligands showed that intrinsic fluorescence at 343 nm was enhanced by up to ∼35% by an authentic phosphate acceptor pseudouridine; it was not enhanced by uridine, cytidine, or the authentic phosphate donor ATP (Fig. 6*A*). Considering that pseudouridine is not fluorescent under the experimental conditions (Fig. 6*B*), the enhanced fluorescence emission is related to changes in EcPUKI associated with the binding of pseudouridine.

Subsequent experiments indicated that the enhanced fluorescence emission was caused by pseudouridine-induced conformational changes. In the structural transition between unliganded EcPUKI and a binary complex with pseudouridine, the side chain of Trp169 between the small and core domains undergoes large positional displacements, with notable changes in its binding environments (Fig. S4, *A*–*C*). The side chain of Trp169, with disordered density, is in a fully exposed orientation in the unliganded state, although it is buried in the binary complex by conformational changes. Considering that the fluorescence of tryptophan is affected by its binding environment, we evaluated whether Trp169 could serve as a fluorescent probe for conformational changes in EcPUKI. Using a W169A mutant, pseudouridine-dependent fluorescence at 343 nm was enhanced only by ∼13%, compared with

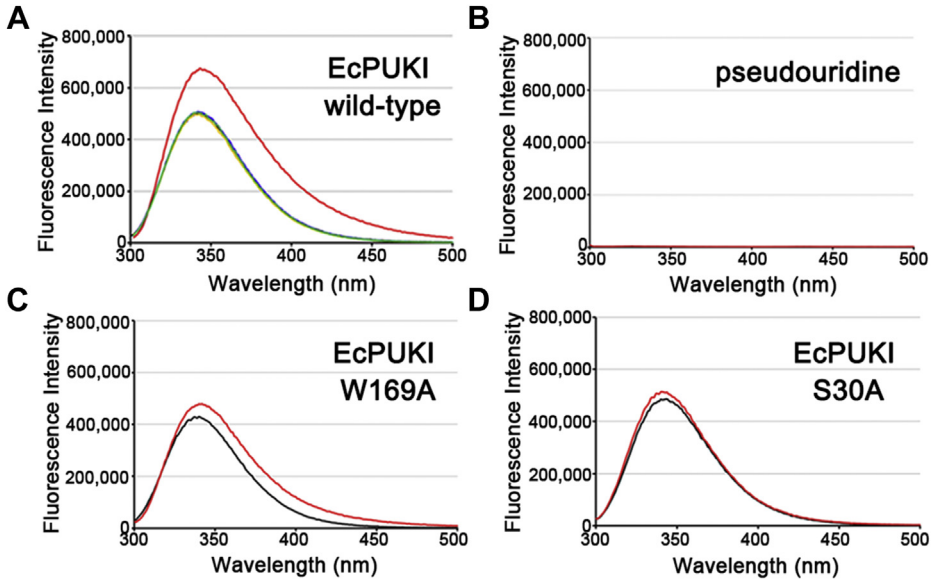

Figure 6. Fluorescence emission spectra of EcPUKIs in the presence of ligands. *A*, emission spectra of wildtype EcPUKI, with an excitation wavelength of 289 nm, in the absence (*black*) and presence of pseudouridine (*red*), uridine (*yellow*), cytidine (*green*), or ATP (*blue*). Maximal intrinsic fluorescence was observed at an emission wavelength of 343 nm. *B*, emission spectrum of pseudouridine at an excitation wavelength of 289 nm. Pseudouridine did not exhibit fluorescence under the experimental conditions. Emission spectra of the (*C*) W169A and (*D*) S30A mutants at an excitation wavelength of 289 nm in the absence (*black*) and presence of pseudouridine (*red*). EcPUKI, pseudouridine kinase from *Escherichia coli* strain B.

the unliganded W169A mutant (Fig. 6*C*). The W169A mutant is catalytically competent; its specific activity and kinetic parameters for pseudouridine are comparable with wildtype EcPUKI (Figs. 5, *A* and *C*, S4*D*). Therefore, Trp169 is a major contributor to the enhanced pseudouridine-dependent fluorescence that is caused by pseudouridine-dependent conformational changes. Pseudouridine did not affect the fluorescence of the S30A mutant (Fig. 6*D*). Consistent with the structural analysis, these findings suggest that the S30A mutant does not undergo conformational changes in solution. Therefore, the pseudouridine-induced conformational changes are required for catalysis by EcPUKI in solution.

Ligand-induced conformational changes and catalysis

The EcPUKI-dependent kinase activity requires ATP as a phosphate donor and pseudouridine as a phosphate acceptor, with cofactors of monovalent and divalent cations. A proposed hydrogen bond between the side-chain hydroxyl group of Ser30 and the N1 of uracil-Ψ in pseudouridine triggers conformational changes *via* the β-stranded small domain.

In a PUKI-dependent kinase reaction, a catalytic base (*e.g.*, $Asp256^{EcPUKI}$) deprotonates O5′ of the ribosyl moiety in pseudouridine (Figs. 3*B* and S5*A*). The resulting deprotonated O5′ of the ribosyl moiety performs a nucleophilic attack on the γ-phosphate group of ATP, thereby producing pseudouridine 5′-monophosphate and ADP. Liberation of the terminal γ-phosphate of ATP requires a catalytic acid. Structural and functional analyses of EcPUKI (this study), AtPUKI (17), and RBSK (21, 24, 26, 27) indicated that the aspartate residue in the immediate vicinity of the O5′ of the ribosyl moiety constituted the catalytic base (Fig. S5, *B*–*D*). However, the catalytic acid is diverse: Lys291 in RBSK from *A. thaliana* (Fig. S5*B*) (24) and possibly a water molecule in the Mg^{2+}-coordinating shell near ATP in AtPUKI (Fig. S5*C*) (17). Our activity and structural analyses identified Asp256 as the catalytic base (Figs. 3*B*, 5, *A* and C). Consistent with a catalytic role for Asp256, the D256A mutant showed a 3280-fold decreased k_{cat} and 1.4-fold increased K_m for ATP (Fig. 5*C*). Moreover, Lys185 in EcPUKI could be located in the vicinity of the γ-phosphate of ATP (Fig. S5*E*) and be crucial for activity (Fig. 5*A*). However, a role for Lys185 as a catalytic acid is controversial; the K185A variant showed a 54-fold increased K_m and 100-fold decreased k_{cat} for ATP (Fig. 5*C*).

We were unable to evaluate the effects of conformational changes on catalysis because a ternary complex of EcPUKI with ATP and pseudouridine is unavailable. However, fluorescence measurements suggested that conformational changes require pseudouridine; ATP was insufficient (Fig. 6*A*). A structural comparison indicated that the conformational changes do not affect the structural integrity of the ATP-binding site in EcPUKI (Fig. S6). The function of pseudouridine-induced conformational changes is unclear; it could include orienting the O5′ of the ribosyl moiety of pseudouridine and the γ-phosphate group of ATP in a position suitable for nucleophilic attack, enhancing affinity for ATP, or providing the catalytic acid. Our structural and kinetic analyses suggest a functional linkage between pseudouridine-dependent conformational changes and catalysis.

Conclusion

We provide structural evidence for pseudouridine-dependent conformational changes of dimeric EcPUKI. Kinetic and fluorescence analyses further indicated that those conformational changes are required for the activity of EcPUKI. Ser30 in the substrate-binding loop of EcPUKI forms a hydrogen bond with a pseudouridine nucleobase, triggering pseudouridine-dependent conformational changes. Therefore, a serine (or threonine) residue in the substrate-binding loop is conserved among PUKI family proteins, as are two key asparagine and lysine residues, which mediate hydrogen bonding with a pseudouridine nucleobase. The presence of the active site residues Asn143 and Lys170 for maintaining the substrate affinity and Ser30 for inducing conformational changes for catalysis provides mechanistic insight into the high fidelity of PUKI for pseudouridine, without disturbing pyrimidine homeostasis.

Experimental procedures

Phylogenetic analysis

BLASTP 2.9.0+ was used to identify homologs of AtPUKI in the UniProtKB/Swiss-Prot Database (https://www.ebi.ac.uk/Tools/sss/ncbiblast/) (18, 28). The top 20 highly homologous proteins were YOW5_SCHPO (pseudouridine-metabolizing bifunctional protein; *Schizosaccharomyces pombe*), PSUK_ECOLI (PUKI; *E. coli*), YEII_ECOLI (uncharacterized sugar kinase YeiI; *E. coli*), RBSK_MOUSE (RBSK; *Mus musculus*), RBSK_LACLA (RBSK; *Lactococcus lactis subsp. lactis*), RBSK_HUMAN (RBSK; *Homo sapiens*), RBSK_DICDI (RBSK; *Dictyostelium discoideum*), RBSK_BACHD (RBSK; *Bacillus halodurans*), RBSK_BACSU (RBSK; *Bacillus subtilis*), RBSK_LEIMA (RBSK; *Leishmania major*), RBSK_SCHPO, RBSK_ARATH (RBSK; *A. thaliana*), RBSK_ECOLI, RBSK_ECO57 (RBSK; *E. coli* O157:H7), HLDE_BLOPB (bifunctional HldE; *Blochmannia pennsylvanicus*), HLDE_VIBCB (bifunctional HldE; *Vibrio campbellii*), HLDE_BRADU (bifunctional HldE; *Bradyrhizobium diazoefficiens*), HLDE_SHEB8 (bifunctional HldE; *Shewanella baltica*), K1PF_XANCP (1-phosphofructokinase; *Xanthomonas campestris pv. campestris*), and INGK_EXIAC (guanosine–inosine kinase; *Exiguobacterium acetylicum*).

To identify regions with two active site residues in the homolog proteins, homology modeling was performed using SWISS-MODEL (https://swissmodel.expasy.org/) (19). MSA was conducted for the amino acid sequences of the regions using the R package "msa" (20). Next, the squared root of the pairwise distance was calculated by the method "identity" of the R package "seqinr" (29). Finally, clustering for phylogenetic tree construction was performed by neighbor-joining method implemented in the R package "ape" (30).

Cloning and purification of EcPUKI

The PUKI gene from *E. coli* strain B (National Center for Biotechnology Information reference sequence: WP_001208132.1) was amplified by polymerase chain reaction. The

resulting amplification product was cloned into a modified pET28b vector (Merck) that contained a tobacco etch virus protease cleavage site. The vector harboring the gene for EcPUKI and an N-terminal His-tag was transformed into *E. coli* BL21 (DE3) cells. The cells were grown at 37 °C in Luria–Bertani medium until an absorbance of 0.5 at 600 nm. Recombinant EcPUKI was then induced with 0.5 mM IPTG for 16 h at 20 °C. The *E. coli* cells were harvested, suspended, and sonicated in buffer A (50 mM Tris–HCl at pH 8.0, 300 mM KCl, and 5% [w/v] glycerol). Recombinant EcPUKI with an N-terminal His-tag was purified by immobilized metal affinity chromatography using a HisTrap HP column (GE Healthcare) equilibrated with buffer A and subsequently eluted with buffer A plus 0.5 M imidazole. The N-terminal His-tag was removed by treatment with tobacco etch virus protease overnight at 4 °C. EcPUKI was further subjected to size-exclusion chromatography on a Superdex 200 column (GE Healthcare) equilibrated with buffer A.

The mutants for structural and functional analyses were constructed using mutagenic primers (Table S1). Vector construction and protein purification were performed as described previously. CD measurements of several enzymes, including wildtype EcPUKI and the S30A, N143A, W169A, and K170A mutants, indicate that mutations do not cause global structural perturbations (Fig. S7). To form a binary complex with pseudouridine, EcPUKI was purified with buffer B (50 mM potassium phosphate at pH 7.4, 300 mM KCl, and 5% [w/v] glycerol).

Crystallization and structure determination

Tag-free EcPUKI was concentrated to ∼15 mg/ml and then subjected to crystallization using the sitting drop vapor-diffusion method at 22 °C. Initial crystal screening was performed using the commercially available kits. Crystals of unliganded EcPUKI in buffer A were produced in 0.2 M magnesium formate, 18 to 22% PEG 3350, and 5% glycerol. The crystallization of a possible ternary complex was carried out, with ADP and pseudouridine, uridine, or cytidine as a phosphate acceptor. Specifically, EcPUKI in buffer B was reacted at 4 °C with 2 mM ADP and 2 mM ligand of interest for 1 h and then subjected to crystallization. However, these crystallization conditions resulted in a structure with a phosphate acceptor but not ADP. Therefore, we considered these conditions to be sufficient for the binary complex. The crystallization of wildtype EcPUKI with uridine or cytidine and the S30A mutant with pseudouridine was successful under conditions identical to the conditions for the unliganded EcPUKI. However, crystals of wildtype EcPUKI with pseudouridine were produced in 1.0 M lithium chloride, 0.1 M MES (pH 6.0), and 18% PEG 6000. Prior to data collection, crystals for the binary complex with various ligand(s) were soaked in crystallization solution plus 4 mM ADP and 4 mM phosphate acceptor. Even with these soaking experiments, the enzyme formed a binary complex only with a phosphate acceptor. Cryoprotection was achieved using 20% glycerol plus crystallization solution.

Diffraction data collection was conducted at 100 K with a 0.5° oscillation angle on beamlines 7A and 11C at the Pohang Accelerator Laboratory. The collected data were indexed, integrated, and scaled using HKL2000 program (31). The high-resolution cutoff was based on a $CC_{1/2}$ statistical value of approximately 0.4 (32, 33). All crystals belonged to the space group *P3*, with four monomers in the asymmetric unit, except for the EcPUKI–pseudouridine complex, which contained eight monomers in an asymmetric unit of the space group $P2_1$.

The structure of unliganded wildtype EcPUKI was solved by molecular replacement using Phaser in PHENIX program (34), with the structure of a putative sugar kinase from *Clostridium perfringens* (PDB ID: 3KZH; sequence identity, 34%) as a search model. The initial model was manually rebuilt and refined using COOT (35) and PHENIX, respectively. Initial refinement by PHENIX yielded a model with a high R_{work} and an R_{free} value of >30%. At this stage, only residues or regions of the model with a reasonable electron density were included into the working structure. Subsequent cycles of PHENIX with anisotropic *B*-factor refinement were performed with incorporation of more residues. Cycles of refinement and extensive model rebuilding improved the structure by reducing the R_{work} and R_{free} values. At that stage, the refined model of unliganded EcPUKI was used as a search model for the molecular replacement of binary complexes with uridine, cytidine, or pseudouridine. In the middle of refinement, uridine, cytidine, and pseudouridine were present in the structure based on the *Fo–Fc* map of the active site. The data collection and refinement statistics are provided in Table 1. In the EcPUKI–pseudouridine complex, two of eight monomers had highly disordered features, possibly leading to a high R_{free} value (Table 1). MolProbity (36) in PHENIX program was used for structure validation.

Activity assay

N-terminal His-tagged enzymes were purified in buffer A by immobilized metal affinity chromatography as described previously and subjected to desalting on a HiPrep 26/10 (GE Healthcare) with buffer A.

Two different assays, a direct assay (37) and an enzyme-coupled assay (14, 24, 38), were employed to measure EcPUKI activity, as reported previously for the assays of AtPUKI (17). In the direct assay, the reaction mixture contained 40 mM Tris–HCl (pH 7.5), 20 mM divalent cation, 50 mM monovalent cation, 0.003% phenol red, 4 mM ATP, and 95 nM wildtype EcPUKI. After 2 min of incubation at 25 °C, the enzyme reaction was triggered by adding 1.25 mM pseudouridine, and absorbance at 430 nm was monitored for 30 s. The monovalent cations tested were LiCl, NaCl, KCl, RbCl, and CsCl, and the divalent cations were $MgCl_2$, $MnCl_2$, and $CaCl_2$. The phosphate donor candidates were ATP, GTP, CTP, and UTP at 1 mM. All assays were conducted in triplicate.

In the enzyme-coupled assay, the reaction mixture consisted of 40 mM Tris–HCl (pH 7.5), 20 mM $MgCl_2$, 50 mM KCl, 0.2 mM NADH, 2 mM phosphoenolpyruvate, the indicated concentrations of EcPUKI, 18 to 28 units of lactate dehydrogenase and 12 to 20 units of pyruvate kinase per milliliter, and pseudouridine or ATP as the substrates. After 2 min of

incubation at 25 °C, the enzyme reaction was initiated by adding the remaining substrate, and the decrease in absorbance at 340 nm was monitored. The initial velocity was determined between 15 and 45 s and expressed as the corresponding ADP concentration change per minute, using an extinction coefficient of 6220 M^{-1} cm^{-1} at 340 nm for NADH. Sigmaplot (Systat Software) was used to calculate the K_m and V_{max}.

Fluorescence measurement

Fluorescence spectra were collected at room temperature from 1.0 mg/ml N-terminal His-tagged EcPUKI and mutants using the QuantaMaster 400 (Horiba-PTI). The emission spectra of EcPUKIs were obtained at an excitation wavelength of 289 nm. For fluorescence measurement in the presence of ligand(s), EcPUKI was incubated at 4 °C for 4 h with 312.5 μM nucleoside (pseudouridine, uridine, or cytidine) or 750 μM ATP.

Data availability

The atomic coordinates and structural factors have been deposited in the PDB (http://www.rcsb.org) under ID code 7VTD, 7VTE, 7VTF, 7VTG, and 7VVA.

Supporting information—This article contains supporting information (17, 24, 39).

Acknowledgments—We thank Jeongyun Lee for her assistance in the purification of enzyme for CD measurements. This work was supported by the National Research Foundation of Korea grant funded by the Korea government (Ministry of Science and ICT) (grant nos.: 2020R1A4A1018890 and 2021R1A2C2092118 [to S. R.]) and Basic Science Research Program funded by the Ministry of Education (grant no.: 2021R1A6A1A10044950 [to D. P.]).

Author contributions—S.-H. K., M. K., D. P., S. B., and S. R. formal analysis; S.-H. K., M. K., and S. B. investigation; S.-H. K., M. K., D. P., S. B., and S. R. visualization; S.-H. K., M. K., D. P., S. B., and S. R. writing-original draft; D. P. and S. R. supervision.

Conflict of interest—The authors declare that they have no conflicts of interest with the content of this article.

Abbreviations—The abbreviations used are: AtPUKI, PUKI from *Arabidopsis thaliana*; EcPUKI, PUKI from *Escherichia coli* strain B; EcRBSK, RBSK of *Escherichia coli*; MSA, multiple sequence alignment; PDB, Protein Data Bank; PfkB, phosphofructokinase B; PUKI, pseudouridine kinase; RBSK, ribokinase.

References

1. Roundtree, I. A., Evans, M. E., Pan, T., and He, C. (2017) Dynamic RNA modifications in gene expression regulation. *Cell* **169**, 1187–1200
2. Frye, M., Harada, B. T., Behm, M., and He, C. (2018) RNA modifications modulate gene expression during development. *Science* **361**, 1346–1349
3. Charette, M., and Gray, M. W. (2000) Pseudouridine in RNA: What, where, how, and why. *IUBMB Life* **49**, 341–351
4. Helm, M. (2006) Post-transcriptional nucleotide modification and alternative folding of RNA. *Nucleic Acids Res.* **34**, 721–733
5. Zaccara, S., Ries, R. J., and Jaffrey, S. R. (2019) Reading, writing and erasing mRNA methylation. *Nat. Rev. Mol. Cell Biol.* **20**, 608–624
6. Wang, X., Zhao, B. S., Roundtree, I. A., Lu, Z., Han, D., Ma, H., Weng, X., Chen, K., Shi, H., and He, C. (2015) N(6)-methyladenosine modulates messenger RNA translation efficiency. *Cell* **161**, 1388–1399
7. Eyler, D. E., Franco, M. K., Batool, Z., Wu, M. Z., Dubuke, M. L., Dobosz-Bartoszek, M., Jones, J. D., Polikanov, Y. S., Roy, B., and Koutmou, K. S. (2019) Pseudouridinylation of mRNA coding sequences alters translation. *Proc. Natl. Acad. Sci. U. S. A.* **116**, 23068–23074
8. Carlile, T. M., Rojas-Duran, M. F., Zinshteyn, B., Shin, H., Bartoli, K. M., and Gilbert, W. V. (2014) Pseudouridine profiling reveals regulated mRNA pseudouridylation in yeast and human cells. *Nature* **515**, 143–146
9. Schwartz, S., Bernstein, D. A., Mumbach, M. R., Jovanovic, M., Herbst, R. H., León-Ricardo, B. X., Engreitz, J. M., Guttman, M., Satija, R., Lander, E. S., Fink, G., and Regev, A. (2014) Transcriptome-wide mapping reveals widespread dynamic-regulated pseudouridylation of ncRNA and mRNA. *Cell* **159**, 148–162
10. Spenkuch, F., Motorin, Y., and Helm, M. (2014) Pseudouridine: Still mysterious, but never a fake (uridine)! *RNA Biol.* **11**, 1540–1554
11. Gilbert, W. V., Bell, T. A., and Schaening, C. (2016) Messenger RNA modifications: Form, distribution, and function. *Science* **352**, 1408–1412
12. Chen, M., Urs, M. J., Sánchez-González, I., Olayioye, M. A., Herde, M., and Witte, C. P. (2018) m(6)A RNA degradation products are catabolized by an evolutionarily conserved N(6)-Methyl-AMP deaminase in plant and mammalian cells. *Plant Cell* **30**, 1511–1522
13. Breitman, T. R. (1970) Pseudouridulate synthetase of Escherichia coli: Correlation of its activity with utilization of pseudouridine for growth. *J. Bacteriol.* **103**, 263–264
14. Preumont, A., Snoussi, K., Stroobant, V., Collet, J. F., and Van Schaftingen, E. (2008) Molecular identification of pseudouridine-metabolizing enzymes. *J. Biol. Chem.* **283**, 25238–25246
15. Chen, M., and Witte, C. P. (2020) A kinase and a glycosylase catabolize pseudouridine in the peroxisome to prevent toxic pseudouridine monophosphate accumulation. *Plant Cell* **32**, 722–739
16. Park, J., and Gupta, R. S. (2008) Adenosine kinase and ribokinase–the RK family of proteins. *Cell Mol. Life Sci.* **65**, 2875–2896
17. Kim, S. H., Witte, C. P., and Rhee, S. (2021) Structural basis for the substrate specificity and catalytic features of pseudouridine kinase from Arabidopsis thaliana. *Nucleic Acids Res.* **49**, 491–503
18. Altschul, S. F., Madden, T. L., Schäffer, A. A., Zhang, J., Zhang, Z., Miller, W., and Lipman, D. J. (1997) Gapped BLAST and PSI-BLAST: A new generation of protein database search programs. *Nucleic Acids Res.* **25**, 3389–3402
19. Waterhouse, A., Bertoni, M., Bienert, S., Studer, G., Tauriello, G., Gumienny, R., Heer, F. T., de Beer, T. A. P., Rempfer, C., Bordoli, L., Lepore, R., and Schwede, T. (2018) SWISS-MODEL: Homology modelling of protein structures and complexes. *Nucleic Acids Res.* **46**, W296–W303
20. Bodenhofer, U., Bonatesta, E., Horejš-Kainrath, C., and Hochreiter, S. (2015) msa: an R package for multiple sequence alignment. *Bioinformatics* **31**, 3997–3999
21. Sigrell, J. A., Cameron, A. D., Jones, T. A., and Mowbray, S. L. (1998) Structure of Escherichia coli ribokinase in complex with ribose and dinucleotide determined to 1.8 A resolution: Insights into a new family of kinase structures. *Structure* **6**, 183–193
22. Holm, L., and Laakso, L. M. (2016) Dali server update. *Nucleic Acids Res.* **44**, W351–W355
23. Sigrell, J. A., Cameron, A. D., and Mowbray, S. L. (1999) Induced fit on sugar binding activates ribokinase. *J. Mol. Biol.* **290**, 1009–1018
24. Kang, P. A., Oh, J., Lee, H., Witte, C. P., and Rhee, S. (2019) Crystal structure and mutational analyses of ribokinase from Arabidopsis thaliana. *J. Struct. Biol.* **206**, 110–118
25. Krissinel, E., and Henrick, K. (2007) Inference of macromolecular assemblies from crystalline state. *J. Mol. Biol.* **372**, 774–797
26. Li, J., Wang, C., Wu, Y., Wu, M., Wang, L., Wang, Y., and Zang, J. (2012) Crystal structure of Sa239 reveals the structural basis for the activation of ribokinase by monovalent cations. *J. Struct. Biol.* **177**, 578–582
27. Paul, R., Patra, M. D., and Sen, U. (2015) Crystal structure of apo and ligand bound vibrio cholerae ribokinase (Vc-RK): Role of monovalent cation induced activation and structural flexibility in sugar phosphorylation. *Adv. Exp. Med. Biol.* **842**, 293–307

28. Boutet, E., Lieberherr, D., Tognolli, M., Schneider, M., Bansal, P., Bridge, A. J., Poux, S., Bougueleret, L., and Xenarios, I. (2016) UniProtKB/Swiss-Prot, the manually annotated section of the UniProt KnowledgeBase: How to use the entry view. *Methods Mol. Biol.* **1374**, 23–54
29. Charif, D., and Lobry, J. (2007) SeqinR 1.0-2: A contributed package to the R project for statistical computing devoted to biological sequences retrieval and analysis. In: Bastolla, U., Porto, M., Roman, H., Vendruscolo, M., eds. *Structural Approaches to Sequence Evolution: Molecules, Networks, Populations, Series Biological and Medical Physics, Biomedical Engineering*, Springer Verlag, NY: 207–232
30. Paradis, E., and Schliep, K. (2019) Ape 5.0: an environment for modern phylogenetics and evolutionary analyses in R. *Bioinformatics* **35**, 526–528
31. Otwinowski, Z., and Minor, W. (1997) Processing of X-ray diffraction data collected in oscillation mode. *Methods Enzymol.* **276**, 307–326
32. Karplus, P. A., and Diederichs, K. (2012) Linking crystallographic model and data quality. *Science* **336**, 1030–1033
33. Diederichs, K., and Karplus, P. A. (2013) Better models by discarding data? *Acta Crystallogr. D Biol. Crystallogr.* **69**, 1215–1222
34. Liebschner, D., Afonine, P. V., Baker, M. L., Bunkóczi, G., Chen, V. B., Croll, T. I., Hintze, B., Hung, L. W., Jain, S., McCoy, A. J., Moriarty, N. W., Oeffner, R. D., Poon, B. K., Prisant, M. G., Read, R. J., *et al.* (2019) Macromolecular structure determination using X-rays, neutrons and electrons: Recent developments in phenix. *Acta Crystallogr. D Struct. Biol.* **75**, 861–877
35. Emsley, P., Lohkamp, B., Scott, W. G., and Cowtan, K. (2010) Features and development of coot. *Acta Crystallogr. D Biol. Crystallogr.* **66**, 486–501
36. Chen, V. B., Arendall, W. B., 3rd, Headd, J. J., Keedy, D. A., Immormino, R. M., Kapral, G. J., Murray, L. W., Richardson, J. S., and Richardson, D. C. (2010) MolProbity: All-atom structure validation for macromolecular crystallography. *Acta Crystallogr. D Biol. Crystallogr.* **66**, 12–21
37. Andersson, C. E., and Mowbray, S. L. (2002) Activation of ribokinase by monovalent cations. *J. Mol. Biol.* **315**, 409–419
38. Mallette, E., and Kimber, M. S. (2018) Structural and kinetic characterization of (*S*)-1-amino-2 propanol kinase from the aminoacetone utilization microcompartment of *Mycobacterium smegmatis*. *J. Biol. Chem.* **293**, 19909–19918
39. Robert, X., and Gouet, P. (2014) Deciphering key features in protein structures with the new ENDscript server. *Nucleic Acids Res.* **42**, W320–W324